

First-Principles Determination of Molecular Conformations of Cyclic Adenosine 3',5'-Monophosphate in Gas Phase and Aqueous Solution

Xi Chen^{†,‡} and Chang-Guo Zhan^{*‡}

Key Laboratory of Pesticide and Chemical Biology of the Ministry of Education, College of Chemistry, Central China Normal University, Wuhan 430079, People's Republic of China, and Department of Pharmaceutical Sciences, College of Pharmacy, University of Kentucky, 725 Rose Street, Lexington, Kentucky 40536

Received: July 29, 2008; Revised Manuscript Received: October 21, 2008

Extensive first-principles electronic structure calculations were performed in this study to explore the possible molecular structures and their concentration distribution of an intracellular second messenger, that is, cyclic adenosine 3',5'-monophosphate (cAMP), and its protonated form (cAMPH) in the gas phase and aqueous solution. The calculations resulted in prediction of four different stable conformers of cAMP and eight different stable conformers of cAMPH and their relative Gibbs free energies in the gas phase and aqueous solution. All of the computational results consistently demonstrate that the predominant conformers of cAMP and cAMPH are always the cAMP-chair-*anti* and cAMPH-chair2-*syn* conformers, respectively, in both the gas phase and aqueous solution. It has been demonstrated that the free energy barriers calculated for the intertransformation reactions between different conformers are very low (below ~6 kcal/mol) such that the intertransformation reactions between different conformers are very fast so that the concentration distribution of the system can quickly reach the thermodynamic equilibration during the process of binding with a protein. The calculated phenomenological pK_a of 3.66 is in good agreement with the experimental pK_a of 3.9 reported in literature, suggesting that the computational predictions resulted from this study are reasonable.

Introduction

Cyclic adenosine 3',5'-monophosphate (cAMP, Figure 1) was found to be an important second messenger in early studies of Sutherland and co-workers.¹ It plays important roles in vision, muscle contraction, neurotransmission, exocytosis, and cell growth and differentiation.² cAMP is synthesized from adenosine triphosphate (ATP) by adenylate cyclase located on cell membranes and degraded by a superfamily of enzymes known as phosphodiesterases (PDEs) into AMP. As the concentration of cAMP is elevated, it will activate a cAMP-dependent protein kinase such as protein kinase A (PKA)³ which is ubiquitous in mammalian cells and is a well-characterized member of the serine/threonine protein kinase family. PKA is normally in a catalytically inactive state until it binds with cAMP. The activated PKA can phosphorylate a number of other proteins, which is known to be critical for regulating a multitude of cellular processes including metabolism, gene transcription, ion flux, growth, and cell death.³

There have been considerable interests in the X-ray crystal structures of cAMP in complex with various enzymes to better understand its role in biochemical systems.^{4–21} Summarized in Table 1 are examples of complex structures along with their protein data bank (PDB) identifications (IDs). From Table 1, it can be found that cAMP adopts a chair conformation (for the six-membered ring containing the P atom, see below) in most enzymes except in nucleoside diphosphate kinase and calmodulin-sensitive adenylate cyclase, where cAMP is in boat conformation. When in complex with cAMP-dependent protein kinase, nucleoside diphosphate kinase, or calmodulin-sensitive

adenylate cyclase, the adenylyl group of cAMP is in *syn* conformation (see Figure 1), whereas in other proteins the adenylyl group of cAMP is in *anti* conformation. A ¹H NMR study reported by Groneborn²² indicated that cAMP binds with cAMP-receptor protein (CRP) solely in the *syn* conformation.

Topiol et al. theoretically studied four different conformers of cAMP (see Figure 2) in vacuum, using the semiempirical AM1 quantum mechanical (QM) method to optimize the geometries and Hartree–Fock (HF) method with STO-3G basis set to calculate the energies neglecting solvent effects.²³ Their calculated relative HF/STO-3G//AM1 energies suggested that cAMP prefers to have the chair-*anti* conformation in the gas phase. Kirschner et al.^{24,25} studied the *syn* and *anti* conformations of the chair structure of cAMP anion by performing QM calculations on these two conformers at the AM1, PM3, HF/3-21G*, and HF/6-31G* levels accounting for solvent effects by using Cramer/Truhlar SM2 and SM3 semiempirical methods.^{26,27} These researchers also employed a supermolecule approach to model the hydration of cAMP at the PM3 level. In their supermolecule models, explicit water molecules were added to model the solvent environment of a cAMP molecule. The results obtained by Kirschner et al. suggested that in solution the chair structure of cAMP has a conformational preference of *anti* isomer. Salter et al.²⁸ also studied the relative energies of the chair-*syn* and chair-*anti* conformations of cAMP by carrying out QM calculations using the HF and B3LYP methods with 6-31G* and 6-31+G* base sets. These researchers accounted for the solvent effects by using two continuum solvation models implemented in Gaussian98 program: one is a simple Onsager model which uses a spherical cavity; the other is a more sophisticated isodensity polarization continuum method (IPCM) for final single-point energy calculations. Their results also indicated that the *anti* conformation is more stable than the *syn* by ~6 kcal/mol, which is consistent with the computational

* To whom correspondence should be addressed. E-mail: zhan@uky.edu.
Tel: 859-323-3943. Fax: 859-323-3575.

[†] Central China Normal University.

[‡] University of Kentucky.

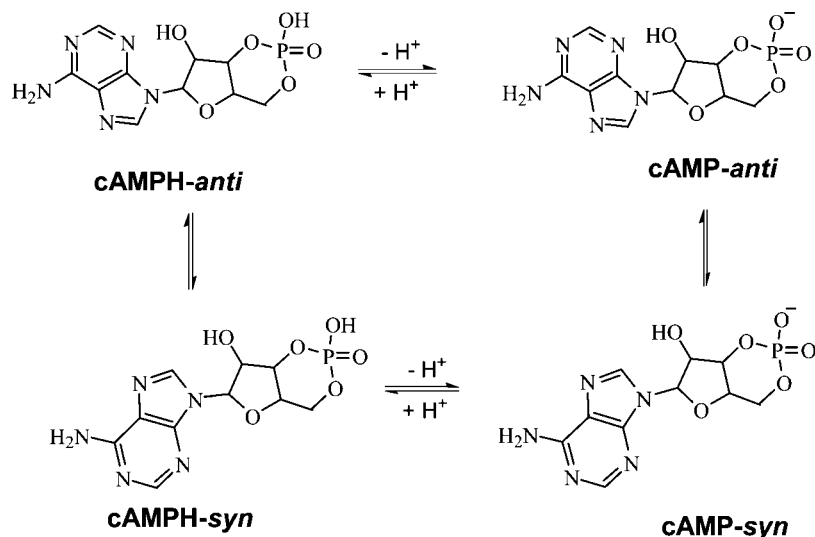


Figure 1. Protonation and conformational changes of intracellular second messenger cAMP in aqueous solution.

TABLE 1: Conformations of cAMP in X-ray Crystal Structures of Various Proteins^a

| enzyme | conformation | ID | ref |
|--|--------------------|------|-----|
| catabolite gene activator protein complex with DNA (Cap-DNA Complex) | chair- <i>anti</i> | 1cgp | 4 |
| cAMP-dependent protein kinase regulatory subunit type II β | chair- <i>syn</i> | 1cx4 | 5 |
| catabolite gene activator protein | chair- <i>anti</i> | 1g6n | 6 |
| catabolite gene activator T127L/S128A | chair- <i>anti</i> | 1hw5 | 7 |
| catabolite gene activator protein -DNA(31–2E) | chair- <i>anti</i> | 1j59 | 8 |
| catabolite gene activator protein--Alphactd-DNA | chair- <i>anti</i> | 1lb2 | 9 |
| dianthin 30 | chair- <i>anti</i> | 1lpc | 10 |
| nucleoside diphosphate kinase | boat- <i>syn</i> | 1nhk | 11 |
| Catabolite Gene Activator Protein -DNA (ICAP38) | chair- <i>anti</i> | 1o3q | 12 |
| catabolite gene activator protein -DNA ([6C,17G]ICAP38) | chair- <i>anti</i> | 1o3r | 12 |
| catabolite gene activator protein-DNA([6C,17G]ICAP38) | chair- <i>anti</i> | 1o3s | 13 |
| GLN181ASP | chair- <i>anti</i> | 1o3t | 12 |
| Catabolite Gene Activator Protein -DNA ([6C,17G]ICAP30) | chair- <i>anti</i> | 1q5o | 14 |
| potassium/sodium hyperpolarization-activated cyclic nucleotide-gated channel 2 | chair- <i>anti</i> | 1q43 | 14 |
| camp dependent protein kinase | chair- <i>syn</i> | 1rgs | 15 |
| catabolite gene activator-DNA | chair- <i>anti</i> | 1run | 16 |
| catabolite gene activator-DNA PHE181GLU | chair- <i>anti</i> | 1ruo | 16 |
| calmodulin-sensitive adenylate cyclase | chair- <i>syn</i> | 1sk6 | 17 |
| hypothetical protein, similar to potassium channel protein | chair- <i>anti</i> | 1vp6 | 18 |
| calmodulin-sensitive adenylate cyclase | boat- <i>syn</i> | 1xfw | 19 |
| adenylate cyclase | chair- <i>anti</i> | 1ykd | 20 |
| catabolite gene activator protein -DNA. | chair- <i>anti</i> | 2cgp | 21 |

^a All crystal structures are taken from the RCSB protein data bank (PDB) via Web site <http://www.rcsb.org/pdb/>.

results reported by Kirschner et al.²⁵ The calculated results are qualitatively consistent with experimental observations,^{29–31} as far as the lowest-energy conformation of cAMP anion is concerned. However, all of the published computational studies accounting for solvent effects have not examined any boat structure of cAMP anion. No computational study has been reported for any structure of the protonated state³² of cAMP (denoted by cAMPH here for convenience), to the best of our knowledge.

We are interested not only in the lowest-energy conformation of cAMP anion, but also in the thermodynamic distribution of all possible conformations of cAMP anion and its protonated state in solution in order to eventually understand how this

important intracellular second messenger interacts with its various receptor proteins and metabolic enzymes (PDEs). It has been demonstrated that the dominant molecular species and conformer in solution is not necessarily the dominant molecular species and conformer in the binding site of a protein.³³ Therefore, all molecular species (protonated or deprotonated) of cAMP and all of their conformers are potentially important for its binding with a protein, regardless of their concentrations in solution. Knowing the concentration distribution of all conformers of both cAMP and cAMPH in solution, one can further theoretically study the possible binding of each molecular species/conformer with a protein and evaluate the microscopic binding free energy. The appropriately combined use of the

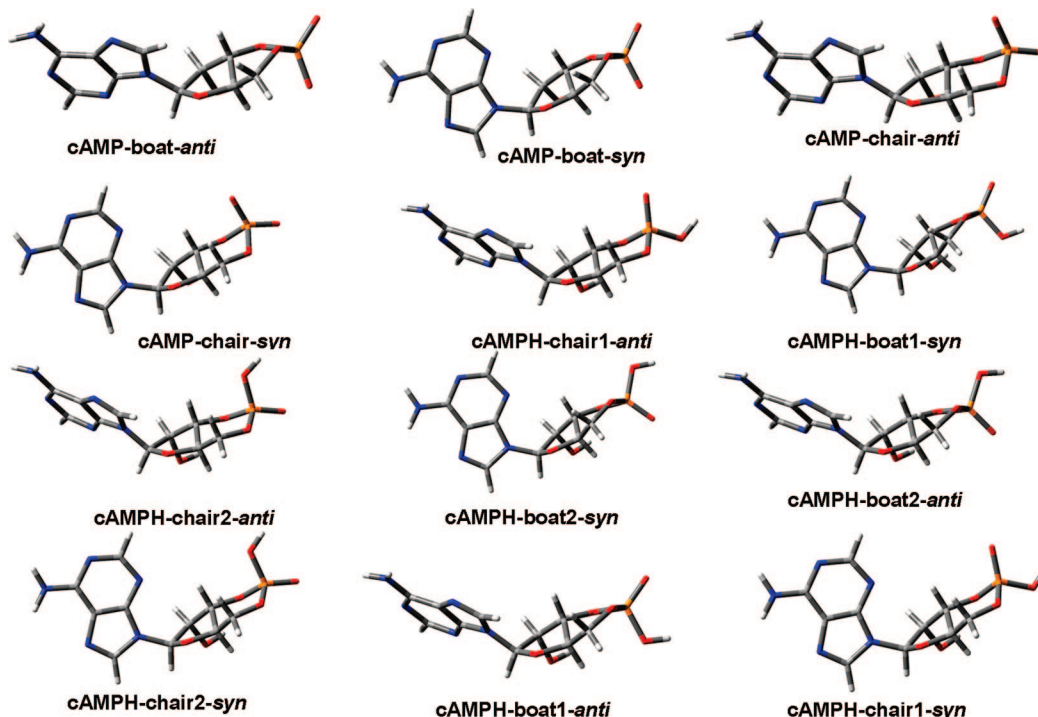


Figure 2. Geometries of various stable conformers of cAMP and cAMPH optimized at the B3LYP/6-31G* level.

calculated microscopic binding free energies and the concentration distribution can lead to prediction of the overall, phenomenological binding free energy for cAMP/cAMPH binding with a protein, as demonstrated in our recent computational studies on nicotinic acetylcholine receptors (nAChRs) binding with multiple molecular species of nicotine and other nAChR agonists.³³

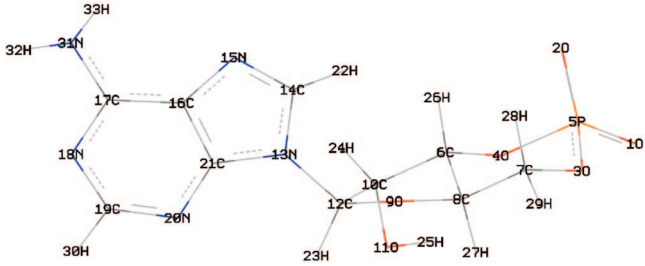
In the present study, all of the possible conformations of cAMP and cAMPH and their relative Gibbs free energies were determined by performing first-principles electronic structure calculations that accurately account for solvent effects. The calculated energetic results enabled us to theoretically predict the concentration distribution of all conformers of cAMP and cAMPH in the gas phase and aqueous solution.

Computational Details. The initial geometries of all cAMP-boat structures were built from the X-ray crystal structure of cAMP-Nucleoside diphosphate kinase¹¹ and the initial geometries of all cAMP-chair structures were from the cAMP-CAP-DNA crystal structure.⁴ The main flexibility of cAMP is associated with the riboside bond (i.e., the rotational angle O9–C12–N13–C14, see Table 2). To explore all possible conformers of cAMP, we performed full 360° rigid potential energy surface scans on these structures with a step size of 15° using Hartree–Fock (HF) method and 6-31G* basis set. Previous theoretical studies have demonstrated that electron correlation effects are not important in geometry optimization. Geometrical parameters optimized using the HF method are quite close to the ones optimized using density functional theory (DFT) or second order Møller–Plesset perturbation theory (MP2) method.³⁴ To further examine this, the geometries optimized at the HF/6-31G* were refined by using gradient-corrected density functional theory (DFT) with B3LYP functional³⁵ and 6-31G* basis set. Four local minima are located on the potential energy surface and the corresponding geometries were used as the corresponding initial ones of boat-syn, boat-anti, chair-syn, and chair-anti conformers (Figure 2). In addition, the geometries of the transition states were also optimized at the B3LYP/6-31G* level.

Further, starting from the initial structures of cAMP conformers, we attached one hydrogen atom to the O1 or O2 atom of each cAMP conformer (see Table 2) to generate the initial structures of cAMPH (Figure 2).

For all conformers in this study, the geometries optimized at the B3LYP/6-31G* level were used to perform the harmonic frequency analysis at the same B3LYP/6-31G* level to make sure that each of the optimized geometries is associated with a local minimum on the potential energy surface and to estimate the thermodynamic corrections to the Gibbs free energy. For the geometries of the transition states, we also carried out the harmonic frequency calculations at the B3LYP/6-31G* level to estimate the thermodynamic corrections to the Gibbs free energies and to confirm that the transition state geometries are indeed associated with the first-order saddle point on the potential energy surface. By using the geometries optimized at the B3LYP/6-31G* level, two theoretical models, that is, DFT using B3LYP functional and MP2 method, in combination with three basis sets, that is, 6-31+G*, 6-31++G**, and 6-311++G**, were employed to perform single-point energy calculations.

The geometries optimized in the gas phase were also used to perform self-consistent reaction field (SCRF) energy calculations in aqueous solution in order to determine the solvent shifts. Florian and Warshel³⁶ performed a manual geometry search in solution along the corresponding gas phase intrinsic reaction coordinate for the hydrolysis of monomethyl phosphate and demonstrated that the contributions of the solvent-induced structural changes to the overall energetics are small and can be safely neglected. The calculated free energies in aqueous solution were taken as the energies calculated at various levels in the gas phase with the B3LYP/6-31G* zero-point and other thermal corrections (at 298 K and 1 atm) plus the corresponding solvent shift determined by the SCRF calculations at the HF/6-31+G* level. A recently developed SCRF method, known as the surface and volume polarizations for electrostatics (SVPE),^{37–41} implemented in GAMESS program,⁴² was used for the SCRF calculations. This SVPE method is also known as the fully polarizable continuum model (FPCM)^{43,44} because

TABLE 2: Torsion Angles (τ) in the Optimized Geometries of Various cAMP and cAMPH Conformers^a


| conformers | $\tau 1^b$ | $\tau 2^b$ | $\tau 3^b$ | $\tau 4^b$ |
|---------------------------|----------------------|-----------------------|----------------------|------------------------|
| cAMP-boat- <i>anti</i> | 44.93 | -74.49 | -40.16 | -144.38 |
| cAMP-boat- <i>syn</i> | -103.50 | 134.46 | -37.47 | -147.21 |
| cAMP-chair- <i>anti</i> | 42.66 | -76.86 | 63.83 | -179.93 |
| | (30.95) ^c | (-88.62) ^c | (57.19) ^c | (-175.50) ^c |
| cAMP-chair- <i>syn</i> | -101.69 | 136.06 | 64.04 | 178.64 |
| cAMPH-boat1- <i>anti</i> | -3.18 | -121.61 | -22.83 | -151.38 |
| cAMPH-boat1- <i>syn</i> | -103.62 | 135.27 | -20.20 | -152.84 |
| cAMPH-boat2- <i>anti</i> | -2.66 | -121.07 | -25.95 | -152.11 |
| cAMPH-boat2- <i>syn</i> | -104.04 | 134.82 | -23.75 | -153.32 |
| cAMPH-chair1- <i>anti</i> | 53.95 | -66.02 | 55.45 | -174.62 |
| cAMPH-chair1- <i>syn</i> | -102.45 | 136.35 | 53.87 | -175.75 |
| cAMPH-chair2- <i>anti</i> | -0.25 | -118.74 | 50.19 | -176.32 |
| cAMPH-chair2- <i>syn</i> | -101.91 | 136.90 | 49.31 | -175.85 |

^a The geometries were optimized at the B3LYP/6-31G* level. ^b $\tau 1$, $\tau 2$, $\tau 3$, and $\tau 4$ represent torsion angle $\tau_{O9-C12-N13-C14}$, $\tau_{C10-C12-N13-C14}$, $\tau_{P5-O3-C7-C8}$, and $\tau_{O3-C7-C8-O9}$, respectively. ^c Experimental data in the X-ray crystal structure from ref 36.

it fully accounts for both surface and volume polarization effects on the solute-solvent electrostatic interaction. Some advantages of the SVPE method over other SCRF methods can be found in our previous reaction field calculations by using various SCRF methods on the energy barriers of a series of carboxylic acid esters⁴¹ and series of phosphodiester including a simplified cAMP model.⁴⁵

All the gas-phase calculations were carried out using Gaussian03 program⁴⁶ on an HP supercomputer (Superdome with 4 nodes and 256 processors) and an IBM X-series Cluster (with 340 nodes and 1,360 processors) at the University of Kentucky Center for Computational Sciences. The SVPE solvation calculations were carried out on a 34-processors IBM Linux cluster and SGI Fuel workstations using the GAMESS program in our own laboratory.⁴²

Results and Discussion

We carried out two sets of energy calculations. One set of energy calculations were performed by using the geometries optimized at the HF/6-31G* level. The other set of energy calculations were performed by using the geometries optimized at the B3LYP/6-31G* level. The two sets of energetic results are very close. Below, we only discuss the results obtained from the calculations using the geometries optimized at the B3LYP/6-31G* level. The results associated with the geometries optimized at the HF/6-31G* level are provided as Supporting Information.

A. Optimized Geometries. Collected in Table 2 are key torsional angles in the optimized geometries of cAMP and cAMPH. In particular, the major difference between the *syn* and *anti* conformers are governed by the torsional angles $\tau_{O9-C12-N13-C14}$ ($\tau 1$) and $\tau_{C10-C12-N13-C14}$ ($\tau 2$) and the main difference between the boat and chair conformers are controlled by torsional angles $\tau_{P5-O3-C7-C8}$ ($\tau 3$) and $\tau_{O3-C7-C8-O9}$ ($\tau 4$). As seen in Table 2, the equilibrium torsional angles $\tau 1$, $\tau 2$, $\tau 3$, and $\tau 4$ for chair-*anti* conformer of cAMP are 42.66, -72.86, 63.83, and -179.93°, respectively.

The corresponding experimental values of $\tau 1$, $\tau 2$, $\tau 3$, and $\tau 4$ are 30.95, -88.62, 57.19, and -1170.50°, respectively, in the X-ray crystal structure of free cAMP (with Na⁺ ion) where each cAMP anion is in chair-*anti* conformation.⁴⁷ The agreement qualitatively supports our computational predictions on the structures of other conformers when experimental data are not available. For all *syn* conformers, the optimized $\tau 1$ and $\tau 2$ values are always ~ 102 – 104° and ~ 134 – 137° , respectively. However, the $\tau 1$ and $\tau 2$ values optimized for cAMP-*anti* conformers are remarkably different from the corresponding $\tau 1$ and $\tau 2$ values optimized for cAMPH-*anti* conformers. The largest difference is more than 40° . The $\tau 3$ values optimized for cAMP-boat conformers are ~ 11 – 20° smaller than the $\tau 3$ values optimized for cAMPH-boat conformers, whereas the $\tau 4$ values optimized for cAMP-boat conformers are $\sim 10^\circ$ larger than the $\tau 4$ values optimized for cAMPH-boat conformers. So the values of $\tau 1$, $\tau 2$, $\tau 3$, and $\tau 4$ have significant changes when cAMP/cAMPH is protonated/deprotonated. The characteristic values of these crucial geometric parameters for cAMP and cAMPH may be valuable for use as references to assign the protonation states (cAMP or cAMPH) of cAMP existing in X-ray crystal structures, since hydrogen atoms cannot be determined by the X-ray diffraction.

Figure 2 gives the optimized geometries of conformers of cAMP and cAMPH. In the structures of chair-*anti* and boat-*anti* of cAMP, the distance between atoms H22 and H26 (see Table 2 for the labels of the atoms) are 2.54 and 2.55 Å, respectively. These distances fall into the range of unfavorable hydrogen-hydrogen interaction. On the other hand, in the *anti* conformation the adenosine group is far away from the phosphate group and decreases the electrostatic interactions between these two groups and thus will compensate the destabilization effect brought by the unfavorable H22-H26 interaction. In the structures of chair-*syn* and boat-*syn*, H22 shifts away from H26 and N20 has a weak interaction with H26. However, in these structures the distance between N20 of the adenosine group and O2 of the phosphoryl group are 5.13 and

TABLE 3: Calculated Relative Gibbs Free Energies (in kcal/mol) of cAMP/cAMPH Conformers Calculated Using Different Theoretical Methods and Basis Sets in the Gas Phase^a

| conformers | MP2 method | | | B3LYP method | | |
|---------------------------|------------|----------|------------|--------------|----------|------------|
| | 6-31+G* | 6-31++G* | 6-311++G** | 6-31+G* | 6-31++G* | 6-311++G** |
| cAMP-boat- <i>anti</i> | 1.75 | 1.71 | 1.75 | 1.81 | 1.76 | 1.83 |
| cAMP-boat- <i>syn</i> | 3.80 | 3.74 | 3.87 | 4.28 | 4.24 | 4.18 |
| cAMP-chair- <i>anti</i> | 0.00 | 0.00 | 0.00 | 0.00 | 0.00 | 0.00 |
| cAMP-chair- <i>syn</i> | 2.70 | 2.72 | 2.75 | 3.07 | 3.09 | 2.90 |
| cAMPH-boat1- <i>anti</i> | 4.17 | 4.23 | 3.88 | 4.01 | 4.03 | 4.02 |
| cAMPH-boat1- <i>syn</i> | 1.41 | 1.42 | 1.37 | 1.22 | 1.23 | 1.21 |
| cAMPH-boat2- <i>anti</i> | 4.05 | 4.07 | 3.80 | 3.87 | 3.85 | 4.00 |
| cAMPH-boat2- <i>syn</i> | 1.26 | 1.24 | 1.27 | 1.02 | 0.99 | 1.14 |
| cAMPH-chair1- <i>anti</i> | 3.80 | 3.79 | 3.67 | 2.46 | 2.51 | 2.85 |
| cAMPH-chair1- <i>syn</i> | 1.02 | 1.02 | 1.08 | 0.95 | 0.94 | 1.07 |
| cAMPH-chair2- <i>anti</i> | 2.49 | 2.49 | 2.30 | 2.50 | 2.51 | 2.60 |
| cAMPH-chair2- <i>syn</i> | 0.00 | 0.00 | 0.00 | 0.00 | 0.00 | 0.00 |

^a The energy calculations were performed at various levels by using geometries optimized at the B3LYP/6-31G* level. Thermal corrections to Gibbs free energies were estimated at the B3LYP/6-31G* level. For each conformer of cAMP, the corresponding relative free energy was calculated by using eq 1. For cAMPH conformers, their relative free energies were calculated by using eq 2.

6.73 Å, which are 2.87 and 2.29 Å shorter than the corresponding distances in chair-*anti* and boat-*anti* conformers, respectively. This implies that in the *syn* conformations of cAMP the repulsion between the adenosine and phosphoryl groups is stronger than that in the *anti* conformations. Because of the same factor, the boat conformations can benefit from relatively weaker interactions between the phosphoryl and adenosine groups (with an N20–O2 distance of 6.7 to 9.0 Å), though they are more tortuous in structure than the chair conformations.

Unlike the conformers of cAMP, the electrostatic repulsive interaction between the adenosine and phosphoryl groups get decreased in cAMPH structures due to the protonation. In the *anti* conformers, H22 moves away from H26 and thus the unfavorable interaction between these atoms diminishes. In cAMPH-*anti* conformer, N20 has a slightly favorable electrostatic attraction with H24 as the N20–H24 distance is 2.70–2.76 Å. The exception is cAMPH-chair1-*anti* conformer, which has an N20–H24 distance of 4.20 Å. Compared to the N20–H24 interactions in *anti* conformers, N20 has a stronger electrostatic attraction with H26 in the *syn* conformers with an internuclear distance of 2.47–2.49 Å.

B. Relative Free Energies of Different Conformers in Gas Phase. We first aimed to determine the relative thermodynamic stability of various conformers of cAMP and cAMPH. To determine the relative thermodynamic stability of various conformers of cAMP and cAMPH, we first calculated the relative free energies of all conformers determined. The relative free energy (in kcal/mol) of each cAMP conformer, denoted by $\Delta G(\text{cAMP-conformer})$, is calculated via

$$\Delta G(\text{cAMP-conf}) = G(\text{cAMP-conf}) - G(\text{cAMP-chair-anti}) \quad (1)$$

In eq 1, $G(\text{cAMP-conf})$ represents the calculated Gibbs free energy of a given cAMP conformer under consideration, whereas $G(\text{cAMP-chair-anti})$ refers to that of the cAMP-chair-*anti* conformer. So, the Gibbs free energy $\Delta G(\text{cAMP-conf})$ of a given conformer is relative to the cAMP-chair-*anti* conformer. Similarly, the relative free energy of each cAMPH conformer, denoted as $\Delta G(\text{cAMPH-conf})$, is calculated via

$$\Delta G(\text{cAMPH-conf}) = G(\text{cAMPH-conf}) - G(\text{cAMPH-chair2-syn}) \quad (2)$$

Summarized in Table 3 are the relative free energies of all the possible conformers of cAMP and cAMPH. Previous calculations demonstrate that electron correlation effects were quite important in final energy calculation and in evaluation of energy profiles of organic reactions of various esters.⁴⁸ Started from this point, two first-principles theoretical methods, MP2 and B3LYP, were chosen for comparison. To test the dependence of final computational results on the used theoretical method and basis set, the geometries optimized at the B3LYP/6-31G* level were used to perform single-point energy calculations at six different levels of theory: MP2/6-31+G*, MP2/6-31++G**, MP2/6-311++G**, B3LYP/6-31+G*, B3LYP/6-31++G**, and B3LYP/6-311++G** level.

A survey of Table 3 reveals that the energy calculations at all the six levels lead to very similar results and consistently predict that chair-*anti* and chair2-*syn* are the most stable conformers among cAMP and cAMPH species, respectively. The six calculation levels produce similar relative free energies; the largest differences caused by different calculation levels do not exceed 0.4 kcal/mol. This indicates that the even most economic B3LYP/6-31+G* level is adequate for prediction of the relative free energies of cAMP and cAMPH conformers. According to the energetic results calculated at the B3LYP/6-311++G** level, the free energy difference between the boat and chair structures in *syn* conformation is 1.1 kcal/mol and the difference in *anti* conformation is 1.8 kcal/mol, which is in agreement with the previous results obtained by Topoil et al. at lower levels of theory.²³

For cAMPH, protonation on two different phosphate oxygen atoms (O1 or O2, see Table 2) lead to two different types of molecular conformations. For convenience, the names of the cAMPH conformers in Figure 2 and Tables 2–4 include “1” or “2” corresponding to the protonation on O1 or O2, respectively. The calculated energetic results show that the difference in the protonation site only has a minor effect on relative Gibbs free energies in the gas phase. The free energy changes due to the difference in the protonation site (O1 or O2) are 0.02–0.1 kcal/mol for the boat conformers and 0.3–1.1 kcal/mol for the chair conformers.

For cAMP, *anti* conformations are about 2.4–2.9 kcal/mol (at the B3LYP/6-311++G** level) lower in Gibbs free energy than the corresponding *syn* conformations. However, at the same level of theory, *anti* conformations for cAMPH are about 1.8–2.9 kcal/mol higher in Gibbs free energy than the corre-

TABLE 4: Calculated Relative Gibbs Free Energies (ΔG , in kcal/mol), Concentration Distribution of cAMP/cAMPH Conformers, and Microscopic pK_a Values of cAMPH Conformers in Aqueous Solution^a

| conformers | ΔG | contribution ^b | pK_a^c |
|---------------------------|------------|---------------------------|----------|
| cAMP-boat- <i>anti</i> | 1.16 | 0.124 | |
| cAMP-boat- <i>syn</i> | 3.00 | 0.006 | |
| cAMP-chair- <i>anti</i> | 0.00 | 0.870 | |
| cAMP-chair- <i>syn</i> | 4.82 | 0.000 | |
| cAMPH-boat1- <i>anti</i> | 1.52 | 0.048 | 2.74 |
| cAMPH-boat1- <i>syn</i> | 0.66 | 0.205 | 3.37 |
| cAMPH-boat2- <i>anti</i> | 3.44 | 0.002 | 1.33 |
| cAMPH-boat2- <i>syn</i> | 2.62 | 0.007 | 1.94 |
| cAMPH-chair1- <i>anti</i> | 2.37 | 0.011 | 2.12 |
| cAMPH-chair1- <i>syn</i> | 2.31 | 0.013 | 2.16 |
| cAMPH-chair2- <i>anti</i> | 1.12 | 0.093 | 3.03 |
| cAMPH-chair2- <i>syn</i> | 0.00 | 0.621 | 3.86 |
| Phenomenological pK_a | | | 3.66 |
| Expt ^d | | | 3.9 |

^a The relative free energy of each conformer (that is, ΔG) in aqueous solution was taken as the sum of single-point energy calculated at the B3LYP/6-311++G**//B3LYP/6-31G* level, thermal corrections to Gibbs free energy estimated at the B3LYP/6-31G* level, solvation free energy calculated with SVPE solvation model at the HF/6-31+G* level, and the nonelectrostatic contributions to solvation free energy estimated with IEFPCM solvation model. Equations 3 and 4 were used for the conformers of cAMP and cAMPH, respectively. ^b The distributions of cAMP/cAMPH conformers in aqueous solution were evaluated by using eq 5. ^c The micro pK_a values were estimated with eq 9, assuming that all cAMPH conformers were converted into cAMP-chair-*anti* conformer after deprotonating. ^d Experimental pK_a of cAMPH from reference.

sponding *syn* conformations. This remarkable difference may be attributed to the repulsive electrostatic interaction between the adenosine and phosphate groups that is significantly stronger for cAMP. The repulsive electrostatic interaction between the adenosine and phosphate groups greatly diminishes in cAMPH due to the protonation of the phosphate group. Compared to the *syn* conformations of cAMP, the *syn* conformations of cAMPH are stabilized by the favorable N20–H24 hydrogen bonding interaction.

C. Conformational Distribution in Aqueous Solution. By using the optimized geometries discussed above, we calculated the solvation free energy of each conformer by using the SVPE method. The relative free energy (in kcal/mol) of a given cAMP conformer, denoted by $\Delta G(\text{cAMP-conf, sol})$, is calculated via

$$\Delta G(\text{cAMP-conf, sol}) = G(\text{cAMP-conf, sol}) - G(\text{cAMP-chair-anti, sol}) \quad (3)$$

in which $G(\text{cAMP-conf, sol})$ and $G(\text{cAMP-chair-anti, sol})$ represent the calculated Gibbs free energies of a given cAMP conformer and the reference conformer (cAMP-chair-*anti*), respectively, in aqueous solution. Similarly, the relative free energy of each cAMPH conformer, denoted by $\Delta G(\text{cAMPH-conf, sol})$, is calculated via

$$\Delta G(\text{cAMPH-conf, sol}) = G(\text{cAMPH-conf, sol}) - G(\text{cAMPH-chair2-syn, sol}) \quad (4)$$

Summarized in Table 4 are relative free energies of the conformers of cAMP and cAMPH in solution. On the basis of the above discussion on the different levels of theory, we used the gas phase free energies obtained from the B3LYP/6-

311++G** calculations and added the SVPE-calculated solvation free energies (solvent shifts) to obtain the final relative free energies in solution. Similar to gas phase, in aqueous solution the cAMP-chair-*anti* and cAMPH-chair2-*syn* are the most stable conformers for cAMP and cAMPH species, respectively. However, cAMP-boat-*syn* becomes the most unstable one among the four conformers in solution, whereas cAMP-chair-*syn* is the most unstable conformer in gas phase.

Compared to the relative free energies calculated in the gas phase, the solvent effects significantly decrease the free energy differences between the *syn* and *anti* cAMPH conformers by 1.0–2.1 kcal/mol, but significantly increase the free energy differences between the O1-protonated cAMPH conformers and the corresponding O2-protonated cAMPH conformers by 1.0–1.9 kcal/mol. Hence, the difference in the protonation site becomes more important for different cAMPH conformers in solution.

On the basis of the relative Gibbs free energies of cAMP/cAMPH conformers in aqueous solution, we estimated the distribution of each conformer within the cAMP or cAMPH species by using the Boltzmann distribution,

$$\frac{N_i}{N} = \frac{e^{-\Delta G_i/kT}}{\sum_j e^{-\Delta G_j/kT}} \quad (5)$$

In eq 5, k is the Boltzmann constant, T is the temperature, ΔG_i represents the relative Gibbs free energies of a conformer under consideration, and N_i/N refers to the relative concentration distribution (fraction) of the conformer within the cAMP or cAMPH species.

As shown in Table 4, for cAMP species the most stable chair-*anti* conformer has ~87% of the concentration distribution. The boat-*anti* conformer has ~12% of the distribution, and the contribution from the other two conformers is negligible. For cAMPH, the chair2-*syn* and boat1-*syn* conformers contribute ~62 and ~20%, respectively, to the total cAMPH concentration. It should be noted that the ratio of the total concentration of all cAMP conformers to the total concentration of all cAMPH conformers is dependent on the pH of the solution. However, the relative concentration distribution of all conformers within a same molecular species (cAMP or cAMPH) is independent of the pH.

D. Intertransformation Reactions between Different Conformers. We are interested in whether one conformer of cAMP (or cAMPH) can easily change to another. The concentration distribution of different conformers can quickly reach a thermodynamic equilibration only when the intertransformation reactions between different conformers are sufficiently fast. The rates of the intertransformation reactions between different conformers are determined by the free energy barriers associated with the reactions. Assuming that the intertransformation reactions between the conformers of the cAMPH species are similar to those between corresponding conformers of the cAMP species, we only studied the intertransformation reactions between the conformers of cAMP. Depicted in Figure 3 are the optimized geometries and the relative free energies of the transition states corresponding to the local-minimum geometries optimized at the same level. In Figure 3, two transition states (TS1 and TS2) are associated with the transformation between the chair-*syn* and chair-*anti* conformers, whereas one transition state (TS3) is associated with the transformation between the boat-*anti* and chair-*anti* conformers of cAMP.

For the transformation between the chair-*syn* and chair-*anti* conformers, TS1 and TS2 are associated with two different

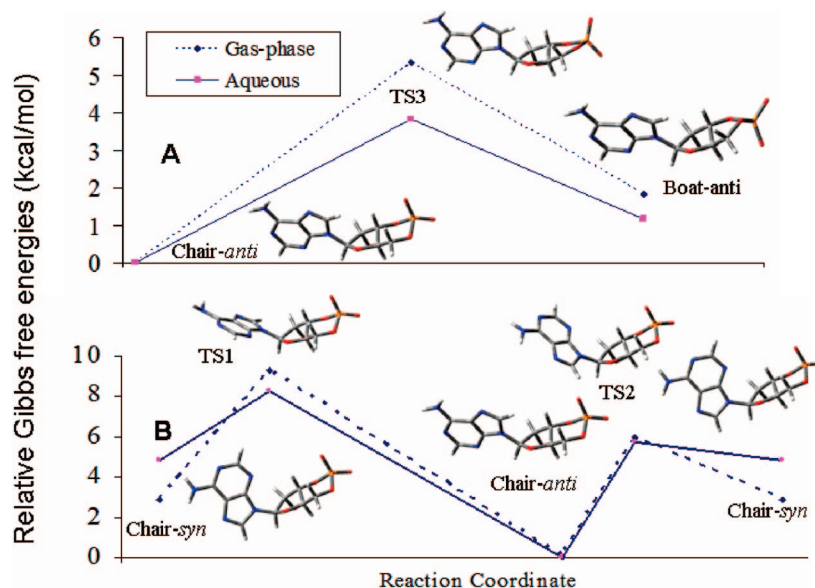


Figure 3. Relative Gibbs free energies in the gas phase and in aqueous solution (A) for the transformation between cAMP-chair-syn and cAMP-chair-anti conformers *via* transition state 1 (TS1) or transition state 2 (TS2), and (B) for the transformation between the cAMP-chair-anti and cAMP-boat-anti *via* transition state 3 (TS3). We used the gas phase free energies obtained from the B3LYP/6-311++G**//B3LYP/6-31G* calculations and added the SVPE-calculated solvation free energies (solvent shifts) to obtain the free energies in solution.

pathways of the transformation. The most favorable transformation pathway is associated with TS2. According to this pathway, the free energy barrier calculated at the B3LYP/6-311++G**//B3LYP/6-31G* level for the transformation from the chair-anti conformer to the chair-syn conformer is only 6.0 kcal/mol in the gas phase and 5.7 kcal/mol in aqueous solution. The free energy barrier calculated at the B3LYP/6-311++G**//B3LYP/6-31G* level for the transformation from the chair-syn conformer to the chair-anti conformer is only 0.9 kcal/mol in the gas phase and 2.8 kcal/mol in the aqueous solution. Similarly, the free energy barriers calculated for the transformation from boat-anti to chair-anti conformer (3.5 kcal/mol in the gas phase and 2.6 kcal/mol in solution) and for the reverse transformation (5.3 kcal/mol in the gas phase and 3.8 kcal/mol in solution) are also very low. The very low free energy barriers mean that the intertransformation reactions between different conformers should be very fast so that the concentration distribution of the system can quickly reach the thermodynamic equilibration. The quick equilibration implies that when a protein favorably binds with just one of the cAMP conformers, the other conformers can quickly transform to the one binding with the protein. Hence, the conformer favorable to a protein is not necessarily the lowest-free-energy conformer in solution, which qualitatively explains why cAMP existed in different conformations in the reported X-ray crystal structures of the different protein-cAMP complexes.

E. Microscopic and Phenomenological pK_a . The pK_a of cAMPH is determined by the Gibbs free energy change in aqueous solution (ΔG_{sol}) of the following protonation process:



The pK_a can be evaluated via

$$pK_a = \Delta G_{\text{sol}} / (2.303RT) \quad (7)$$

Prediction of the free energy change of a protonation process requires knowing the absolute free energy of the proton (H^+)

in aqueous solution, $\Delta G_{\text{hyd}}^{298}(\text{H}^+)$, in addition to the free energies calculated for all of the molecular species mentioned above. Because of the inherent difficulty of measuring absolute solvation free energy of an ion, the reported “experimental” $\Delta G_{\text{hyd}}^{298}(\text{H}^+)$ values have a wide range from -252.6 to -264.1 kcal/mol.⁵⁰ We predicted $\Delta G_{\text{hyd}}^{298}(\text{H}^+)$ (by using a high-level, ab initio method of incorporating a hybrid supermolecule-continuum approach based on the same SVPE procedure used in the present study) to be -262.4 kcal/mol.^{43b} This value was used to calculate Gibbs free energy change for reaction 6 in the present study.

There are eight stable conformers of cAMPH species and each conformer has a distinct microscopic dissociation constant. Assuming all cAMPH conformers were converted into cAMP-chair-anti conformer (the most stable conformer of cAMP) after deprotonation, we were able to calculate a microscopic pK_a for each conformer by using the calculated free energies in aqueous solution. Further, based on the Gibbs free energies calculated for all of the four conformers of cAMP and eight conformers of cAMPH, we calculated the phenomenological pK_a of cAMPH by using the same computational procedure used in our recent computational study^{44a} on phenomenological pK_a of other systems. The calculated microscopic and phenomenological pK_a values are collected in Table 4.

As seen in Table 4, the microscopic pK_a values of cAMPH-boat1-anti, cAMPH-boat1-syn, cAMPH-boat2-anti, cAMPH-boat2-syn, cAMPH-chair1-anti, cAMPH-chair1-syn, cAMPH-chair2-anti, and cAMPH-chair2-syn were predicted to be 2.74, 3.37, 1.33, 1.94, 2.12, 2.16, 3.03, and 3.86, respectively. The calculated phenomenological pK_a of 3.66 is in good agreement with the experimental pK_a of 3.9 reported in literature.³² The good agreement between the predicted phenomenological pK_a and the experimental pK_a suggests that our predicted concentration distribution of the cAMP and cAMPH conformers and the microscopic pK_a values are reasonable.

Conclusion

The geometries of four possible conformers of cAMP and eight possible conformers of cAMPH (which is the protonated

state of cAMP) and their relative Gibbs free energies have been determined by performing first-principles electronic structure calculations at various levels of theory. It has been shown that the solvation significantly affects the relative free energies of the different conformers. Nevertheless, all of the computational results consistently demonstrate that the predominant conformers of cAMP and cAMPH are always the cAMP-chair-*anti* and cAMPH-chair2-*syn* conformers, respectively, in both the gas phase and aqueous solution. The computationally determined intertransformation reaction pathways and the corresponding free energy barriers indicate that the free energy barriers calculated for the intertransformation reactions between different conformers are very low, suggesting that the intertransformation reactions between different conformers are very fast so that the concentration distribution of the system can quickly reach the thermodynamic equilibration during the process of binding with a protein. The calculated phenomenological pK_a of 3.66 is in good agreement with the experimental pK_a of 3.9 reported in literature, suggesting that our predicted concentration distribution of the cAMP and cAMPH conformers, as well the microscopic pK_a values of various cAMPH conformers, are reasonable.

Acknowledgment. The research was supported in part by Kentucky Science & Engineering Foundation (Grant KSEF-925-RDE-008) and National Natural Science Foundation of China (Grants 20602014, 20503008, and 20372023). The authors also acknowledge the Center for Computational Sciences (CCS) at University of Kentucky for supercomputing time on HP supercomputer (Superdome with 4 nodes and 256 processors) and IBM X-series Cluster (with 340 nodes and 1,360 processors).

Supporting Information Available: Three tables for results calculated by using geometries optimized at the HF/6-31G* level. This material is available free of charge via the Internet at <http://pubs.acs.org>.

References and Notes

- (1) Sutherland, E. W.; Rall, T. W. *J. Biol. Chem.* **1958**, *232*, 1065.
- (2) Callahan, S. M.; Cornell, N. W.; Dunlap, P. V. *J. Biol. Chem.* **1995**, *270*, 17627.
- (3) Walsh, D. A.; Glass, D. B.; Mitchell, R. D. *Curr. Opin. Cell Biol.* **1992**, *4*, 241.
- (4) Schultz, S. C.; Shields, G. C.; Steitz, T. A. *Science* **1991**, *253*, 1001.
- (5) Diller, T. C.; Madhusudan; Xuong, N. H.; Taylor, S. S. *Structure* **2001**, *9*, 73.
- (6) Passner, J. M.; Schultz, S. C.; Steitz, T. A. *J. Mol. Biol.* **2000**, *304*, 847.
- (7) Chu, S. Y.; Tordova, M.; Gilliland, G. L.; Gorshkova, I.; Shi, Y.; Wang, S.; Schwarz, F. P. *J. Biol. Chem.* **2001**, *276*, 11230.
- (8) Parkinson, G.; Wilson, C.; Gunasekera, A.; Ebright, Y. W.; Ebright, R. H.; Berman, H. M. *J. Mol. Biol.* **1996**, *260*, 395.
- (9) Benoff, B.; Yang, H.; Lawson, C. L.; Parkinson, G.; Lui, J.; Blatter, E.; Ebright, Y. W.; Berman, H. M.; Ebright, R. H. *Science* **2002**, *297*, 1562.
- (10) Kurinov, I. V.; Rajamohan, F.; Uckun, F. M. *Arzneim. Forsch.* **2004**, *54*, 692.
- (11) Williams, R. L.; Oren, D. A.; Munoz-Dorado, J.; Inouye, S.; Inouye, M.; Arnold, E. *J. Mol. Biol.* **1993**, *234*, 1230.
- (12) Chen, S.; Vojtechovsky, J.; Parkinson, G. N.; Ebright, R. H.; Berman, H. M. *J. Mol. Biol.* **2001**, *314*, 63.
- (13) Chen, S.; Gunasekera, A.; Zhang, X.; Kunkel, T. A.; Ebright, R. H.; Berman, H. M. *J. Mol. Biol.* **2001**, *314*, 75.
- (14) Zagotta, W. N.; Olivier, N. B.; Black, K. D.; Young, E. C.; Olson, R.; Gouaux, J. E. *Nature* **2003**, *425*, 200.
- (15) Su, Y.; Dostmann, W. R.; Herberg, F. W.; Durick, K.; Xuong, N. H.; Ten Eyck, L.; Taylor, S. S.; Varughese, K. I. *Science* **1995**, *269*, 807.
- (16) Parkinson, G.; Gunasekera, A.; Vojtechovsky, J.; Zhang, X.; Kunkel, T. A.; Berman, H.; Ebright, R. H. *Nat. Struct. Biol.* **1996**, *3*, 837.
- (17) Guo, Q.; Shen, Y.; Zhukovskaya, N. L.; Florian, J.; Tang, W. J. *J. Biol. Chem.* **2004**, *279*, 29427.
- (18) Clayton, G. M.; Silverman, W. R.; Heginbotham, L.; Morais-Cabral, J. H. *Cell* **2004**, *119*, 615.
- (19) Shen, Y.; Zhukovskaya, N. L.; Guo, Q.; Florian, J. *EMBO J.* **2005**, *24*, 929.
- (20) Martinez, S. E.; Bruder, S.; Schultz, A.; Zheng, N.; Schultz, J. E.; Beavo, J. A.; Linder, J. U. *Proc. Natl. Acad. Sci. U.S.A.* **2005**, *102*, 3082.
- (21) Passner, J. M.; Steitz, T. A. *Proc. Nat. Acad. Sci. U.S.A.* **1997**, *94*, 2843.
- (22) Gronenborn, A. M.; Clork, G. M.; Blazy, B.; Baudras, A. *Febs Lett.* **1981**, *136*, 160.
- (23) Topiol, S.; Morgan, T. K., Jr; Sabio, M.; Lumma, W. C., Jr. *J. Am. Chem. Soc.* **1990**, *112*, 1452.
- (24) Kirschner, K. N.; Shields, G. C. *J. Mol. Struct.* **1996**, *362*, 297.
- (25) Kirschner, K. N.; Sherer, E. C.; Shields, G. C. *J. Phys. Chem.* **1996**, *100*, 3293.
- (26) Cramer, C. J.; Truhlar, D. J. *J. Comput.-Aided Mol. Des.* **1992**, *6*, 629.
- (27) Cramer, C. J.; Truhlar, D. J. *J. Comput. Chem.* **1992**, *13*, 1089.
- (28) Salter, E. A.; Wierzbicki, A.; Sperl, G.; Thompson, W. J. *Struct. Chem.* **2003**, *14*, 527.
- (29) Lavalley, D. K.; Zeltmann, A. H. *J. Am. Chem. Soc.* **1974**, *96*, 5552.
- (30) Barry, C. D.; Martin, D. R.; Williams, R. J. P.; Xavier, A. V. *J. Mol. Biol.* **1974**, *84*, 491.
- (31) Lee, C.-H.; Sarma, R. H. *J. Am. Chem. Soc.* **1976**, *98*, 3541.
- (32) Goldberg, R. N.; Tewari, Y. B. *J. Chem. Thermodyn.* **2003**, *35*, 1809.
- (33) (a) Huang, X.; Zheng, F.; Crooks, P. A.; Dwoskin, L. P.; Zhan, C.-G. *J. Am. Chem. Soc.* **2005**, *127*, 14401. (b) Huang, X.; Zheng, F.; Chen, X.; Crooks, P. A.; Dwoskin, L. P.; Zhan, C.-G. *J. Med. Chem.* **2006**, *49*, 7661.
- (34) Zheng, F.; Zhan, C. G.; Ornstein, R. L. *J. Chem. Soc., Perkin Trans. 2* **2001**, *2*, 1.
- (35) (a) Becke, A. D. *J. Chem. Phys.* **1993**, *98*, 5648. (b) Lee, C.; Yang, W.; Parr, R. G. *Phys. Rev. B* **1988**, *37*, 785. (c) Stephens, P. J.; Devlin, F. J.; Chabalowski, C. F.; Frisch, M. J. *J. Phys. Chem.* **1994**, *98*, 11623.
- (36) Varughese, K. I.; Lu, C. T.; Kartha, G. J. *Am. Chem. Soc.* **1982**, *104*, 3398–3401.
- (37) Chang, N.-Y.; Lim, C. J. *Am. Chem. Soc.* **1998**, *120*, 2167.
- (38) Zhan, C.-G.; Bentley, J.; Chipman, D. M. *J. Chem. Phys.* **1998**, *108*, 177.
- (39) Zhan, C.-G.; Chipman, D. M. *J. Chem. Phys.* **1998**, *109*, 10543.
- (40) Zhan, C.-G.; Chipman, D. M. *J. Chem. Phys.* **1999**, *110*, 1611.
- (41) Zhan, C.-G.; Landry, D. W.; Ornstein, R. L. *J. Phys. Chem. A* **2000**, *104*, 7672.
- (42) Schmidt, M. W.; Baldrige, K. K.; Boatz, J. A.; Elbert, S. T.; Gordon, M. S.; Jensen, J. H.; Koseki, S.; Matsunaga, N.; Nguyen, K. A.; Su, S. J.; Windus, T. L.; Dupuis, M.; Montgomery, J. A. *J. Comput. Chem.* **1993**, *14*, 1347.
- (43) (a) Zhan, C.-G.; Niu, S.; Ornstein, R. L. *J. Chem. Soc., Perkin Trans. 2* **2001**, *1*, 23. (b) Zhan, C.-G.; Dixon, D. A. *J. Phys. Chem. A* **2001**, *105*, 11534. (c) Dixon, D. A.; Feller, D.; Zhan, C.-G.; Francisco, J. S. *J. Phys. Chem. A* **2002**, *106*, 3191. (d) Zheng, F.; Zhan, C.-G.; Ornstein, R. L. *J. Phys. Chem. B* **2002**, *106*, 717. (e) Zhan, C.-G.; Dixon, D. A. *J. Phys. Chem. A* **2002**, *106*, 9737. (f) Zhan, C.-G.; Dixon, D. A.; Sabri, M. I.; Kim, M.-S.; Spencer, P. S. *J. Am. Chem. Soc.* **2002**, *124*, 2744. (g) Zhan, C.-G.; Dixon, D. A. *J. Phys. Chem. A* **2003**, *107*, 4403. (h) Zhan, C.-G.; Dixon, D. A.; Spencer, P. S. *J. Phys. Chem. B* **2003**, *107*, 2853. (i) Dixon, D. A.; Feller, D.; Zhan, C.-G.; Francisco, S. F. *Int. J. Mass Spectrom.* **2003**, *227*, 421.
- (44) (a) Lu, H.-T.; Chen, X.; Zhan, C.-G. *J. Phys. Chem. B* **2007**, *111*, 10599. (b) Xiong, Y.; Zhan, C.-G. *J. Phys. Chem. A* **2006**, *110*, 12644. (c) Zhan, C.-G.; Deng, S.-X.; Skiba, J. G.; Hayes, B. A.; Tschampel, S. M.; Shields, G. C.; Landry, D. W. *J. Comput. Chem.* **2005**, *26*, 980. (d) Huang, X.; Zheng, F.; Crooks, P. A.; Dwoskin, L. P.; Zhan, C.-G. *J. Am. Chem. Soc.* **2005**, *127*, 14401. (e) Xiong, Y.; Zhan, C.-G. *J. Org. Chem.* **2004**, *69*, 8451. (f) Chen, X.; Zhan, C.-G. *J. Phys. Chem. A* **2004**, *108*, 3789–3797. (g) Zhan, C.-G.; Dixon, D. A. *J. Phys. Chem. A* **2004**, *108*, 2020.
- (45) Chen, X.; Zhan, C.-G. *J. Phys. Chem. A* **2004**, *108*, 6407.
- (46) Frisch, M. J.; Trucks, G. W.; Schlegel, H. B.; Scuseria, G. E.; Robb, M. A.; Cheeseman, J. R.; Montgomery, J. A., Jr.; Vreven, T.; Kudin, K. N.; Burant, J. C.; Millam, J. M.; Iyengar, S. S.; Tomasi, J.; Barone, V.; Mennucci, B.; Cossi, M.; Scalmani, G.; Rega, N.; Petersson, G. A.; Nakatsuji, H.; Hada, M.; Ehara, M.; Toyota, K.; Fukuda, R.; Hasegawa, J.; Ishida, M.; Nakajima, T.; Honda, Y.; Kitao, O.; Nakai, H.; Klene, M.; Li, X.; Knox, J. E.; Hratchian, H. P.; Cross, J. B.; Adamo, C.; Jaramillo, J.; Gomperts, R.; Stratmann, R. E.; Yazyev, O.; Austin, A. J.; Cammi, R.; Pomelli, C.; Ochterski, J. W.; Ayala, P. Y.; Morokuma, K.; Voth, G. A.; Salvador, P.; Dannenberg, J. J.; Zakrzewski, V. G.; Dapprich, S.; Daniels, D.; Strain, M. C.; Farkas, O.; Malick, D. K.; Rabuck, A. D.; Raghavachari, K.; Foresman, J. B.; Ortiz, J. V.; Cui, Q.; Baboul, A. G.; Clifford, S.; Cioslowski, J.; Stefanov, B. B.; Liu, G.; Liashenko, A.; Piskorz, P.; Komaromi, I.; Martin, R. L.; Fox, D. J.; Keith, T.; Al-Laham, M. A.; Peng, C. Y.; Nanayakkara, A.; Challacombe, M.; Gill, P. M. W.; Johnson, B.; Chen, W.; Wong, M. W.; Gonzalez, C.; Pople, J. A. *Gaussian 03*, revision A.1; Gaussian, Inc.: Pittsburgh, PA, 2003.

(47) Varughese, K. I.; Lu, C. T.; Kartha, G. *J. Am. Chem. Soc.* **1982**, *104*, 3398.

(48) (a) Zhan, C.-G.; Landry, D. W.; Ornstein, R. L. *J. Am. Chem. Soc.* **2000**, *122*, 1522. (b) Zhan, C.-G.; Landry, D. W.; Ornstein, R. L. *J. Am. Chem. Soc.* **2000**, *122*, 2621.

(49) Goldberg, R. N.; Tewari, Y. B. *J. Chem. Thermodyn.* **2003**, *35*, 1809.

(50) Meijias, J. A.; Lago, S. *J. Chem. Phys.* **2000**, *113*, 7306.

JP806702D